10-1-2024

BIOLUMINESENCE-INDUCED PHOTOREDOX CATALYSIS AND ITS MECHANISMS

Dominic Jeffrey Bates
Rowan University

BIOLUMINESENCE-INDUCED PHOTOREDOX CATALYSIS AND ITS MECHANISMS

by

Dominic Jeffrey Bates

A Thesis

Submitted to the
Department of Chemistry and Biochemistry
College of Science and Mathematics
In partial fulfillment of the requirement
For the degree of
Master of Science in Pharmaceutical Sciences
at
Rowan University
July 2, 2024

Thesis Chair: Lark J. Perez, Ph.D., Professor, Department of Chemistry and Biochemistry

Committee Members:
Jonnalagadda Subash, Ph.D., Professor, Head of the Department of Chemistry and Biochemistry
Kandalam Ramanujachary, Ph.D., Professor, Department of Chemistry and Biochemistry
Gustavo Moura-Letts, Ph.D., Professor, Department of Chemistry and Biochemistry
Michael Law, Ph.D., Associate Professor, Department of Biochemistry and Molecular Biology at Stockton University

Dedications

To my family and to Lainie, thank you for sticking with me through everything and for loving me always.

Acknowledgments

I cannot even begin to describe the thanks I have for my professor for the invaluable help and guidance I have received throughout my journey as a graduate student. Additionally, without my defense committee, I would never have been able to venture forth into the world before me without their knowledge and expertise.

I would also like to thank my family and loved ones for their endless moral support, advice, and phone calls to keep me moving and motivated each and every day. Without their faith in me I would not be where I am today.

Abstract

Dominic Jeffrey Bates
BIOLUMINESENCE-INDUCED PHOTOREDOX CATALYSIS AND ITS MECHANISMS
2021-2024
Lark J. Perez, Ph.D.
Master of Science in Pharmaceutical Sciences

The bioluminescence-induced photoredox reaction (BIPR) is a novel methodology developed to overcome the limitations of photo-induced chemistry by initiating chemical work using bioluminescent *Escherichia coli* as a photon source. In industry, photochemistry is superseded by thermochemical reaction processes. Despite its massive potential, there are very few applications in industry for photochemistry. Unlike thermochemistry, reaction scale-ups are not as easy as simple dimensional increases in a reaction vessel due to the nature of light. This deficiency is seemingly overcome through the development of flow technologies; however, the overall yield of such methods remains incomparable with those utilizing thermochemistry. This thesis focuses on a reaction method we have developed to fulfill the requirements for an environmentally friendly, feasible reaction process that could potentially be scaled up in industry. Insights from the data collected provide a deeper understanding of the limitations, strengths, and forces that drive photochemistry that have been achieved via the proposed methodology described therein.

Table of Contents

Table of Contents (Continued)

List of Figures

Figure Page

List of Figures (Continued)

Figure Page

Chapter 1

Introduction

Fossil fuels are a finite source of energy and result in emissions that harm our environment and contribute to global warming. Energy that is both sustainable and renewable provides a solution to a safer and more promising future for our planet. The most plentiful and environmentally friendly energy source in the world is solar energy. To better comprehend this relatively untapped source of power, scientists have calculated that the amount of light irradiating the earth each hour exceeds the energy consumed worldwide for an entire year. [1] Thus, the ability to convert and properly utilize this source is essential.

Fundamentally, light is particle, known as a photon, that moves at light speed. To take advantage of solar energy, certain materials can be used to harvest these fast-moving photons to generate individual electrons and holes. Photovoltaic cells and certain batteries make use of this concept to convert solar energy into electricity. As electricity is not capable of being stored and applied to larger scale applications, the other method for this process would be the conversion of light into chemical energy. This process mimics that of photosynthesis,[1] and theoretically allows for reaction scale-up on an industry level beyond what is capable of from the solar to electric energy conversion process. The reaction process of converting solar energy into chemical energy itself is made possible via the use of a photoredox system. Specifically, what this system entails is the utilization of a catalyst to absorb photons and convert their energy into chemical work. Even more specifically, photocatalysts must be used to harness the photons generated from visible

light which then allows the catalyst to undergo a single-electron-transfer (SET) process with organic substrates.[2] In order to reach this point photocatalysts must first be sufficiently irradiated from a photon that exceeds the catalyst's bandgap. A bandgap can be summarized as the minimum energy required to excite an electron into a state where it can participate in conduction. The smaller the bandgap, the less energy is required to allow for electronic conductivity. Similarly, a narrow bandgap determines whether a catalyst acts as a semiconductor, or if the material has an extremely small or lack of a bandgap, it would be classified as a conductor.

Once a catalyst is irradiated, the excited electron travels from the catalyst's valence band to its conduction band. In simple terms, the valence band is the furthest orbital of a particle in a catalyst in which electrons reside. With this information in mind, the conduction band could be described as the orbitals in which electrons can jump up to with when energized, putting the catalyst in an excited state. Once the electron is promoted to the conduction band, the lack of an electron in the valence band causes an electron-hole pair to form. The combination of an electron-hole pair and excited electron from here allows for catalysts to participate in SET, which produces radicals from water and oxygen in solution that are capable of chemical work. An example of this process can be seen in Figure 1. While the conduction and valence band can both theoretically participate in and contribute to a photoredox system, for the new and novel experiments conducted in this work, the mechanism of action was evaluated.

Figure 1

Overview of a Photoredox System

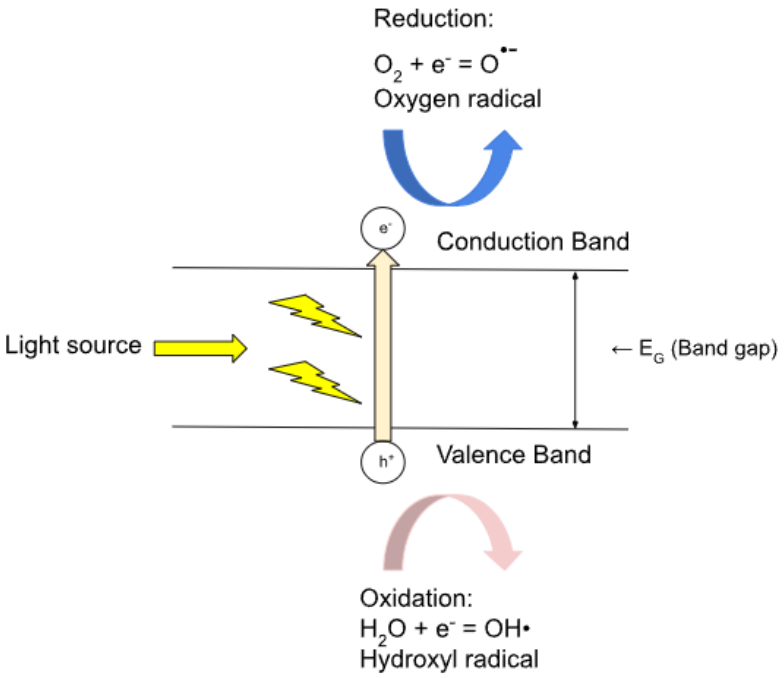

In the context of mimicking solar energy, the sun can be replaced with sources of light powered by electricity, such as LEDs or other lightbulbs. Exploiting the light energy produced from these sources has primarily been conducted utilizing homogeneous catalysts such as ruthenium or iridium-based transition metal catalysts.[1-3] Despite the advantages of such catalysts, my thesis research makes use of graphitic carbon nitride (GCN), an organic semiconductor heterogeneous catalyst. GCN can be produced from the facile polymerization of cyanamide, dicyanamide, or melamine in a tube furnace and boasts advantages over homogenous catalysts due to its ease of separation from solution, higher stability from its polymeric structure, and recyclability for future reactions.[4] More

importantly, however, GCN as an organic catalyst allows for biocompatibility with microorganisms, a factor that ultimately led to the implementation of GCN into our novel reaction, bioluminescence-induced photoredox reaction (BIPR).

Bacteria as a Light Source

BIPR itself is the novel concept of using bioluminescent bacteria as a light source for photoredox reactions. Specifically, light-producing *Escherichia coli* were implemented as our source of light in our photoredox system. In nature, all types of bioluminescent bacteria rely on three essential substrates to produce light; reduced flavin mononucleotide ($FMNH_2$), oxygen, and a long-chain saturated aliphatic aldehyde.[5] Ultimately, *E. coli* was selected for BIPR due to the its compatibility with the *ilux* operon. Bacterial bioluminescence is known to be weak in comparison to other luciferases due to its reliance in nature to the *lux* operon. However, with the *ilux* operon, bacterial light production increases sevenfold. This increased bioluminescent output was characterized by Gregor et. al to allow for single cell imaging of bacteria over several days, highlighting the optimization of light production in single bacterial cells.[6] With this augmented operon, bioluminescence is also only capable of occurring in metabolically active cells,[6] providing the most ideal environment for bacterially mediated photoredox under normal, aerobic conditions.

To understand the employed *ilux* operon, it is essential to understand the original *lux* operon (*luxCDABE(G)*). When expressed, the LuxAB operon codes for luciferase, a heterodimer, that oxidizes long-chain fatty acids into an acid that results in the emission of light. [6, 7] This dimer makes use of the reduced FMN created by the FMN reductase

expressed by the LuxG operon.[7] Subsequently, the aldehyde is generated by a fatty acid reductase complex coded for by LuxCDE.[7] The subsequent light released from this enzymatic cascade results in a wavelength emission around 490 nm (Figure 2).[7]

The expression of the *ilux* operon itself is induced by introducing a plasmid to our *E. coli* bacteria in conjunction with an ampicillin resistance gene. This method allowed for our research group to cultivate bacterial colonies expressing bioluminescence on lysogeny broth (LB) agar plates containing 50 µg/mL of ampicillin, which ensures the only viable bacterial growth present on plates would be for colonies with a resistance to ampicillin and displaying bioluminescence.[6]

Figure 2

Diagram Showing how Bacteria Produce Light

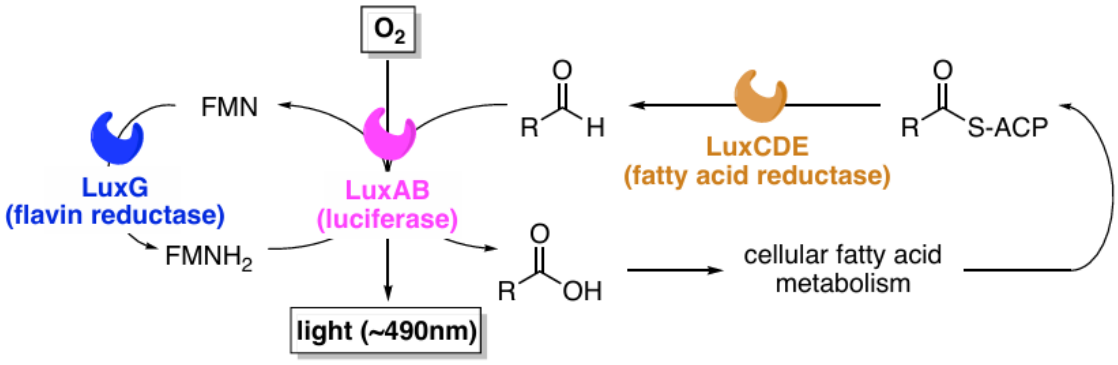

Note. This series of reactions produces a photon of light (~490nm) from a single oxygen molecule.

Bioluminescence-Induced Photoredox Reactions

By using light-producing *E. coli* in a reaction, we could theoretically overcome limitations from traditional light sources by having a source of light homogenously distributed throughout the reaction vessel. In doing so, we could maximize the efficiency of the catalyst within the total volume of the reaction. In systems using an external light source, the efficiency of a catalyst's ability to absorb photons is lessened by the Beer-Lambert-Bouguer law (Beer's Law). In short, light is only capable of penetrating a few millimeters into a reaction vessel due to the distance of the light source from the vessel. Solutions to overcome this issue include lightbulb immersion within the reaction vessel as well as various flow technologies. However, these methodologies still struggle with Beer's Law restricting the amount of light capable of penetrating solution from the surface of the light source. We hypothesize that bioluminescent bacteria can trigger efficient photocatalysis of organic substrates while simultaneously overcoming Beer's Law.

Beginnings of BIPR

For BIPR to occur, a biocompatible catalyst was needed that could drive photoredox reactions. Careful screening for a biocompatible photocatalyst was conducted with a host of catalysts (e.g. Rose Bengal, Eosin Y, $Ru(bpy)_3BArF$), but revealed that bulk (or pristine) GCN was the most suitable for our goal. All other catalysts that one would expect to be the best options for photoredox were found to inhibit bacterial growth and luminescence, and in some cases, outright bacterial death (Figure 3). Historically, GCN is known for its desirable bandgap (2.7 eV), high stability, and easy route of

preparation.[3, 8] While also being capable of splitting water into H_2 and O_2, reducing CO_2, degradation of water pollutants, and a role in wastewater treatment,[8] GCN was found to have an impressive framework in photocatalytic applications. As an organic semiconducting polymer, GCN was thus deemed as the idyllic catalyst for all future studies.

Figure 3

Graph Showing the Biocompatibility of Selected Photocatalysts With Bacteria

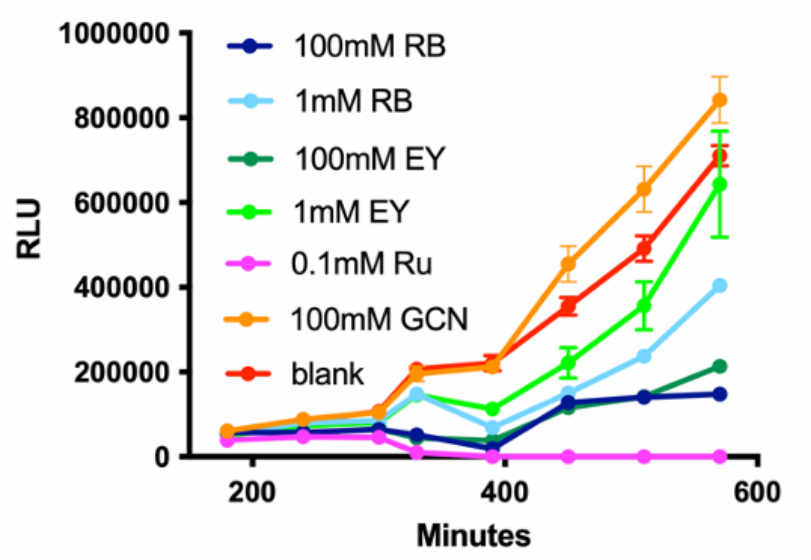

Note. Catalysts were assessed for biocompatibility with *Escherichia coli* over 400 minutes (RB = rose bengal; EY = eosin Y; Ru = $Ru(bpy)_3BArF$; GCN = graphitic carbon nitride). The evaluations are representative of the average of three replicates with error bars representing 95% confidence intervals. Error bars were not shown for the experiments most significantly inhibited RLU (relative light units; luminescence/OD_{600}) for clarity.

Attempted Organic Transformations Using BIPR

Subsequent experiments focused on finding a suitable substrate compatible with our bacteria. Using tetrahydroisoquinalone and various benzylamines, I attempted to use BIPR to complete an organic synthesis route (Figure 4).

Figure 4

Early Synthetic Routes Explored for BIPR

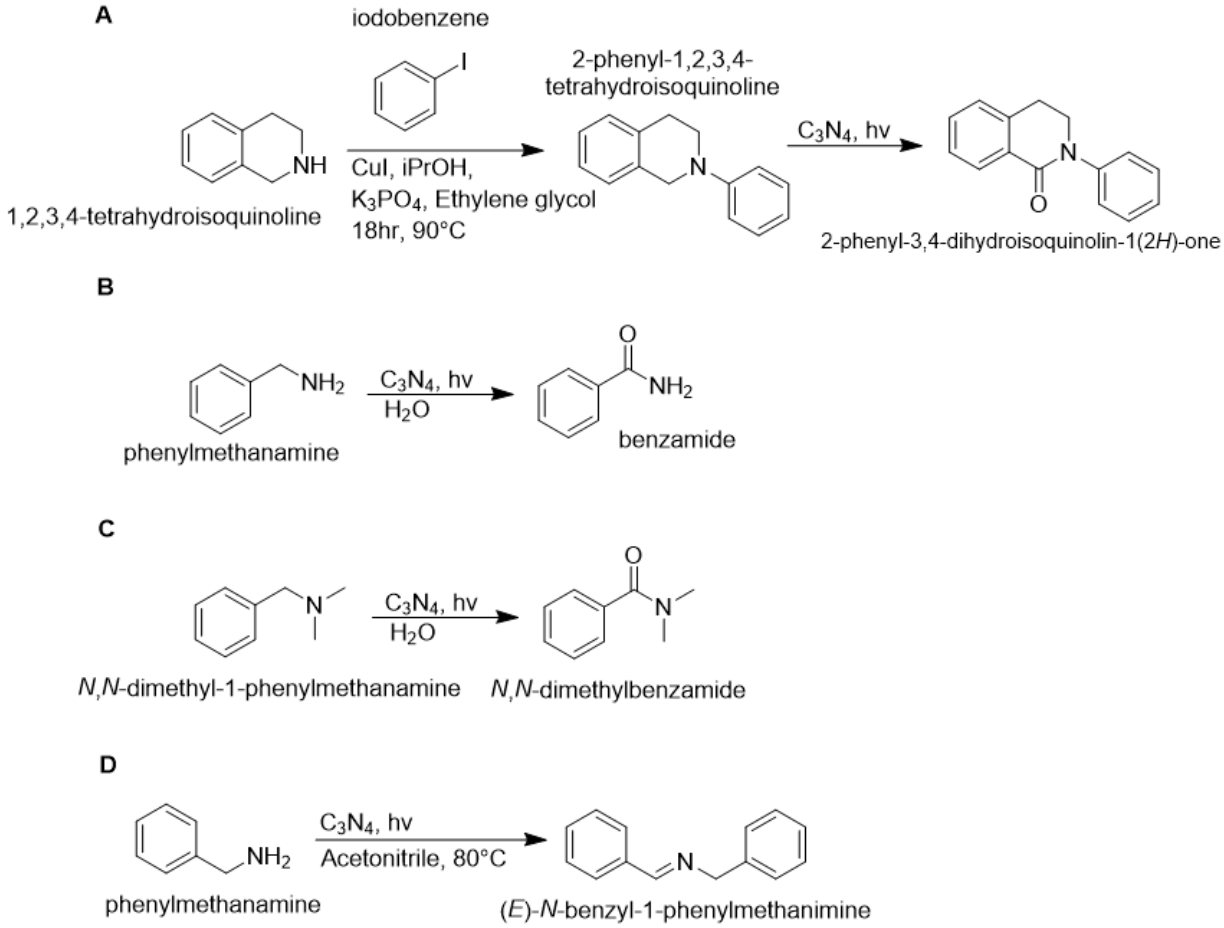

The first route (Figure 4A) involved converting 1,2,3,4-tetrahydroisoquinoline (1,2,3,4-THQ) into 2-phenyl-1,2,3,4-tetrahydroisoquinoline (2-phenyl-THQ). This product would then be placed into a BIPR reaction to form the oxidized product of 2-phenyl-3,4-dihydroisoquinolin-1(2H)-one. To a standard 20mL scintillation vial, 40mg of copper iodide and 850mg of anhydrous potassium phosphate were added to 2mL of isopropyl alcohol. Subsequently, 0.22mL of ethylene glycol was added, along with 0.4mL of 1,2,3,4-THQ. Then, 0.22mL of iodobenzene was inserted via syringe. The resulting solution was then heated to 90°C and allowed to stir for 24h. The organic layer was then extracted with diethyl ether, dried, and ran through a Biotage® flash purification system to isolate 2-phenyl-THQ. This product was then suspended in 1M of DMSO and transferred to the 250mL conical BIPR flask with rigorous exclusion of external light. After running BIPR for 24h, the organic layer was extracted and purified. All resulting crude ^{1}H-NMR data from each run supports that this product was not attained (Appendix A).

Before committing to further BIPR runs, as with the THQ experiments, we decided to test all further BIPR runs on a smaller scale and without bacteria. As a preliminary method in testing the viability of a reaction for use in BIPR, I utilized a 150W Chromalux brand incandescent light bulb as a light source. This lightbulb would then be placed 2.5 cm from a standard 20 mL scintillation vial containing the reaction mixture. This process would allow us to quickly determine the feasibility of a reaction before committing to the lengthy process of bacterial culture for BIPR.

With the failure to produce the oxidized product from THQ, I sought to oxidize phenylmethanamine and N, N-dimethyl-1-phenylmethanamine (Figure 4B and Figure

4C) using the incandescent light bulb as a source of light. Into a standard 20mL scintillation vial I added 20mL of water and 50mg of bulk GCN for each synthetic route. Prior to the initiation of light, I added 100mg each of phenylmethanamine and N, N-dimethyl-1-phenylmethanamine into their respective scintillation vials and left each for 24h, while stirring, with exposure to the lightbulb. The generated crude ^{1}H -NMR results displayed a lack of product for both runs, showing a failure for the oxidation of benzylamines under these conditions (Appendix B and Appendix C).

As a final attempt for an attempted lightbulb-driven organocatalysis, I attempted to oxidatively couple benzylamine hydrochloride (Figure 4D). Into a standard 20mL scintillation vial I added 1mmol of benzylamine hydrochloride into 10mL of acetonitrile with 50mg of bulk GCN. The vessel was then stirred with exposure to the 150W incandescent lightbulb with time points taken at 3.5, 12, and 24h. Crude ^{1}H -NMR results displayed a failure to procure the desired product (Appendix D).

When evaluating the results of each crude NMR for the previous experiments, the program ChemDraw® was used to confirm the presence of the desired final products for each synthesis. Particularly, ChemDraw was used to generate theoretical NMR data that allowed us to quickly assess our crude data. Although ChemDraw is not wholly reliable on interpreting NMR data, in conjunction with our knowledge of reading NMR data, our results clearly did not display any trace of the desired products. With this information in mind, another route of action was needed.

Alternative Substrates for BIPR

Degradation of Organic Dyes

Figure 5

The Chemical Structures of Organic Dyes Tested in BIPR

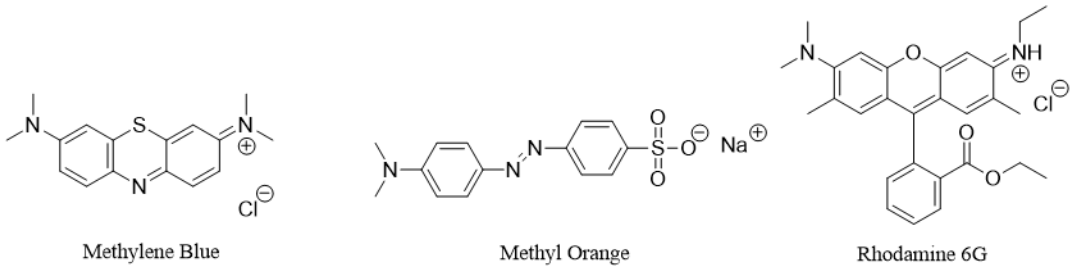

Despite the repeated failures in achieving organic transformations using BIPR, we decided to pursue another route of testing BIPR, the degradation of organic molecules. With suitable precedent for the bleaching of organic dye, we tested the substrates of methylene blue (MB), methyl orange (MO), and rhodamine 6G (R6G) (Figure 5).

Our group decided to test these dyes due to the ease of quantifying remaining dye in solution with GCN via UV-visible spectroscopy. Additionally, each dye was characterized by different ionic properties to further investigate the capabilities of GCN. MB was selected as a cationic dye, R6G as a zwitterionic dye, and MO as an anionic dye. To determine the degradative capacity of GCN we distributed 20mL of each dye (20mg/L) along with 20mg of mpg-GCN catalyst into separate 20mL scintillation vials.

The vials were then placed 2.5cm from our incandescent bulb and were allowed to run for 24h with time points taken every 6h or until complete degradation of the dye (Figure 6).

Figure 6

Testing of Various Organic Dyes Against Bulk-GCN

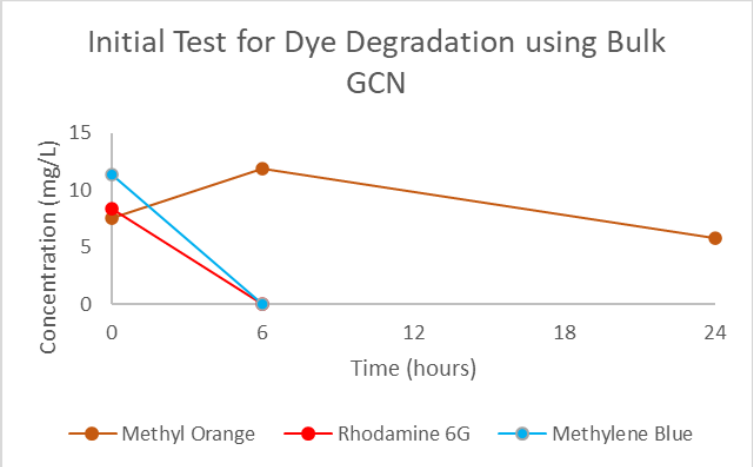

Note. This was a preliminary experiment used to properly determine the ability of each individual dye to be degraded. Despite the lack of a control group, this initial experiment was able to assess the photocatalytic ability of bulk-GCN.

This experiment demonstrates the preferential degradation of MB and R6G while exposing a deficiency in the decomposition of the anionic MO dye. This selective behavior by bulk-GCN provides insight into its surface properties and interactional mechanisms with other potential substrates. More specifically, all data suggests that bulk-GCN is likely to carry a negative surface charge under these experimental conditions.

Active sites on the surface may have a high enough electron density to attract and transfer electrons more strongly with positive or partially positive charged molecules (in the context of cationic and zwitterionic dyes respectively), helping facilitate their adsorption onto the catalyst and subsequent oxidative degradation. The lack of bleaching for the anionic dye implies that MO is either less effectively adsorbed onto the catalyst or is less susceptible to oxidation from bulk-GCN's active sites.

Figure 7

Comparative Graph Between Methylene Blue and Rhodamine 6G Degradation

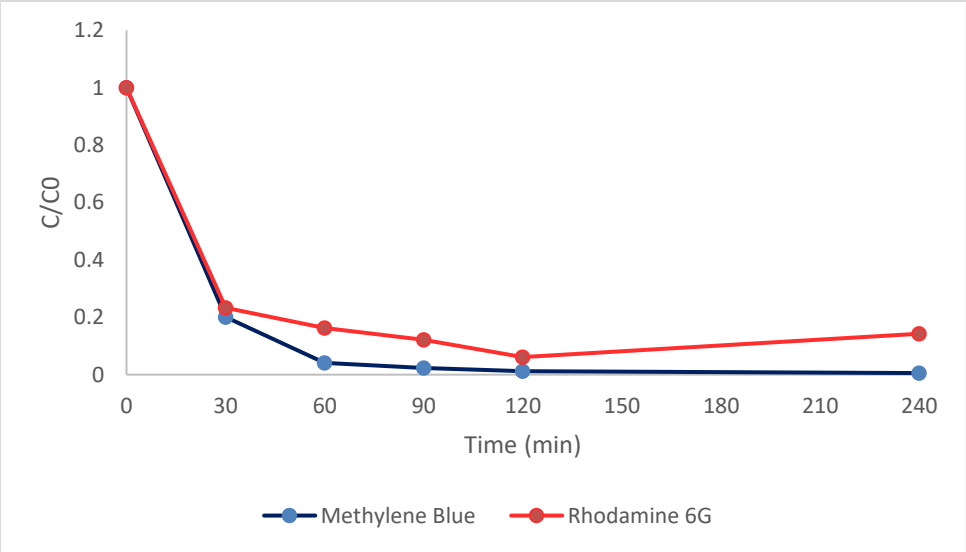

Note. This was another preliminary experiment aimed at comparing the ability of methylene blue and rhodamine 6G to be degraded. Despite the lack of a control group, this experiment was able to identify the dye best suited for further experimentation.

Continuing forward, MB and R6G were further tested in triplicate. This was accomplished by placing 20 mL of each respective dye (20 mg/L) and 20mg of mpg-GCN into 20 mL scintillation vials, using an incandescent lightbulb as a light source (Figure 7). These vials were allowed to run for 4h with time points taken at 0, 30, 60, 90, 120, and 240 minutes. Results show MB's more consistent and marked degradation profile when compared to that of R6G, confirming that MB would be our substrate of choice in a degradation experiment using BIPR.

Degradation of 4-Chlorophenol

Figure 8

The Chemical Structure of 4-Chlorophenol

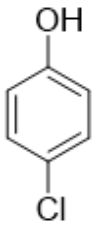

Beyond the bleaching of organic dyes, I decided to attempt to degrade 4-chlorophenol (4-CP) to further test mpg-GCN (Figure 8). Into a 20mL scintillation vial I added 20mg of mpg-GCN into 20mL of 4-CP (20mg/L). Placed 2.5cm away from the 150W Chromalux lightbulb, the vial was then allowed to run for 150 minutes. Time points taken from the scintillation vial were ran through an LCMS to ascertain the concentration of 4-CP over time. Results show a lack of degradation for 4-CP under these

experimental conditions (Figure 9). However, it should be noted that calibration curve data for 4-CP is inconclusive in detecting the concentrations using the LCMS. With this experiment resulting in failure, methylene blue was reaffirmed as our substrate of choice.

Figure 9

Degradation of 4-Chlorophenol Using mpg-GCN

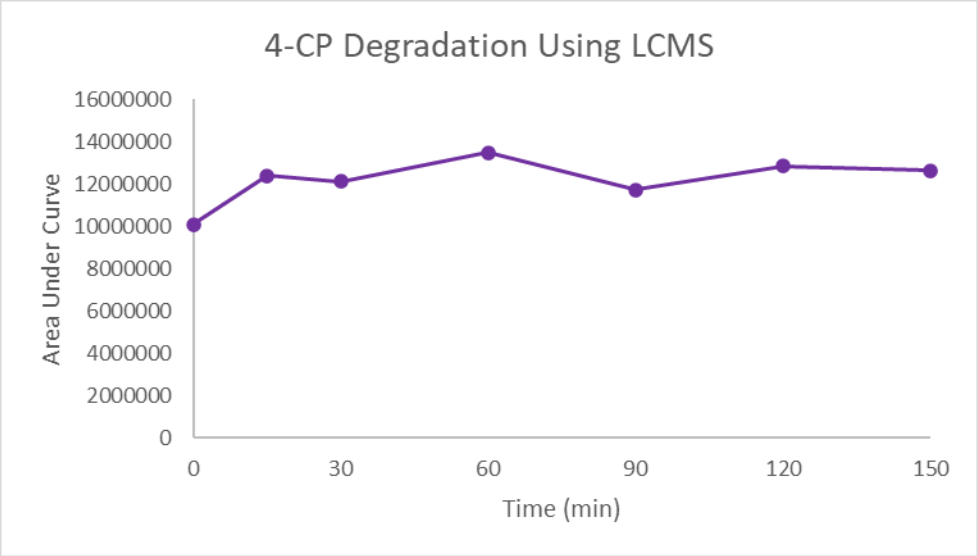

Note. This was a preliminary experiment aimed at determining the ability of 4-chlorophenol to be degraded. Despite the lack of a control group, this initial experiment does not show a marked decrease in 4-chlorophenol concentration as detected by LCMS.

Optimizing GCN

After repeated failures in organic transformations using BIPR, we decided to take advantage of the manipulatable features of bulk GCN. Regardless of our selection of a biocompatible catalyst, we had been unaware of the limitations of bulk GCN. The marked failure of the previously attempted organocatalytic experiments could be characterized by bulk GCN's low surface area, high recombination rate for generated holes, and substandard absorption of visible light.[8] In simpler terms, bulk-GCN's ability for photocatalysis is hindered by a low amount of active sites; the inability to stay energetically active when excited by a photon; and poor absorption of light. Various solutions to these issues include: heteroatom doping, morphological modification, nano-casting, and supramolecular assembly.[8] Each protocol is capable of improving the photocatalytic efficiency of bulk GCN, yet extensive studies demonstrate the ability to finetune the bandgap and optimize the reduction and oxidation potentials for bulk GCN.[9-16]

With an array of modifications possible for GCN, we decided that heteroatom doping stood out as one of the most popular and effective approaches to improving the applicability of GCN.[15] This doping method specifically allowed for modification of the charge density on the surface of GCN, which would result in improved utilization of photons, a more advantageous band gap, and overall significant improvement over bulk GCN. A host of heteroatom-doped catalysts was then made to better refine the BIPR reaction (Figure 10).

Figure 10

The Various Synthetic Routes for Improving GCN

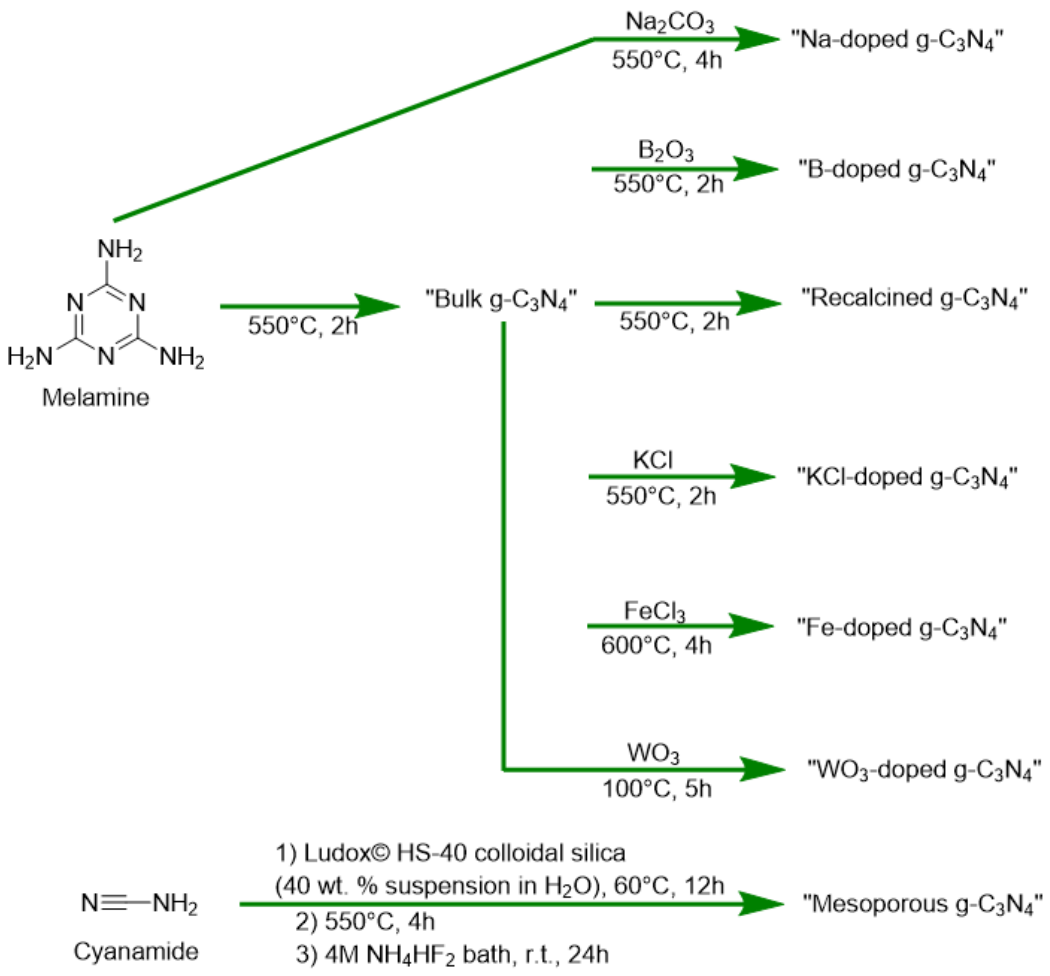

Note. All derivatives of bulk-GCN were calcined using a tube furnace and a ceramic carrying boat.

The primary concern with the heteroatom method was that the introduction of metals within the catalysts would reduce bacterial viability. To circumvent this potential issue, two non-metal "doped" catalysts were prepared.[11, 13]

The first route utilized melamine as a precursor and was used to produce bulk GCN as previously described. The resulting bulk catalyst was then transferred to a porcelain boat and recalcined at 550°C for 2h to produce a supposed mesoporous GCN catalyst that was then ground into fine powder and collected. This catalyst we named "recalcined GCN."

The other route produced a mesoporous GCN using cyanamide as a precursor. Cyanamide was dissolved into a Ludox-HS 40 silica dispersion and dried at 70°C overnight. The resulting gel-like slurry was then moved to a porcelain boat and calcinated at 550°C for 4h under N_2 atmosphere. Afterwards, the sample was washed with a 4 M NH_4HF_2 acid bath that removed the silica template from the catalyst. Finally, the yellow powder produced was washed with water and dried in an aspirator bottle overnight. The dried, yellow powder we named "mesoporous GCN."

In total, we have formulated Na doped [15], boron doped [10], KCl doped [14], iron doped [9], copper doped [16],tungsten doped [12], recalcined [13], and mesoporous GCN (mpg-GCN) [11] (Figure 10). Our array of modified GCN was then assayed to characterize the kinetics and viability for the decomposition of MB. Preliminary kinetics plots from just some of these modified polymers revealed mpg-GCN to have the fastest reaction kinetic with MB (Figure 11). With each heteroatom-doped catalyst (apart from boron doped GCN) showing a slower reaction profile than bulk-GCN, we selected mpg-GCN for implementation into the BIPR reaction. Although the reaction kinetics played a significant role in this decision, the lack of metal ions within mpg-GCN gave us suitable precedent for an increased biocompatibility with bacteria when compared to that of bulk GCN. Additionally, the trend in the heteroatom-doped GCN having lower reaction

kinetics than that of mpg-GCN led us to move forward in experimentation without testing the other catalysts.

Figure 11

Kinetics Plot and Rate Constants for the Decomposition of Methylene Blue in the Presence of Various GCN

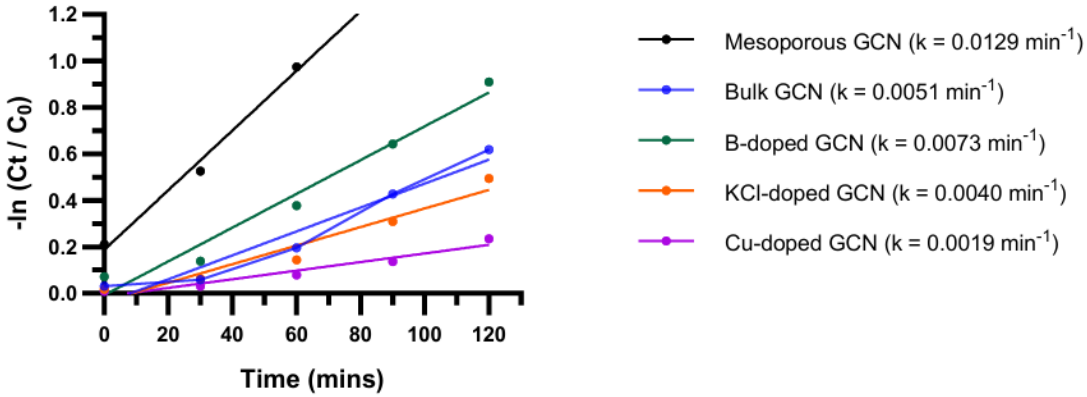

Note. This is a pseudo first order kinetics plot showing the rate constants for the decomposition of methylene blue (20mL of 20mg/L solution in H_2O) with different GCN polymers (2.5mg) irradiated by a 150W full-spectrum incandescent light bulb. Each data point represents the average of three replicates (error bars withheld). C_0 and C respectively represent the initial concentration and concentration at time "t" of methylene blue.

Issues and Solutions to Working with BIPR

Although we had found the proper substrate and catalyst to theoretically allow BIPR to work, unforeseen problems arose as we worked towards developing a proper methodology.

When in solution, GCN is known to adsorb aromatic pollutants to its surface. [10, 11, 15] This is made possible by electrostatic attraction and π–π interactions commonly associated with GCN's tri-*s*-triazine structure. [10, 11, 15] Given that bulk GCN is hindered by its small specific surface area (<10 m^2/g) [15], an important part in determining accessibility to active sites, bulk GCN is not a reliable adsorbent of carbon materials. Heteroatom doping is known to bypass this problem, but as shown previously, biocompatibility with bacteria is still a concern. As a mesoporous catalyst, mpg-GCN is characterized by 2-50 nm pores throughout its structure that lowers its density, increases the surface area, increases active sites, and notably strengthened adsorption ability.[11] While each factor is welcomed in the context of BIPR, the increased adsorptive capability of mpg-GCN resulted in skewing the initial degradation of MB. Experiments utilizing mpg-GCN displayed a marked decrease in MB concentration which was initially attributed to mpg-GCN's desired degradative behavior. However, keeping in mind that non-pristine GCN catalysts have an increased adsorptive function, it was deemed necessary to "equilibrate" catalysts with rigorous exclusion of external light in solution with MB prior to experimental initiation. This allowed us to properly analyze the catalytic ability of GCN while avoiding the misrepresentative "degradation" caused by GCN's adsorptive nature.

Another issue in the process of developing BIPR was the low number of photons produced by our *ilux* expressing *E. coli* culture. The total production of photons possible from our culture was estimated by our group to be ~10^4 photons per cell per second, a low amount especially when compared to that of ~10^{20} photons per second produced by our 150W incandescent light bulb. Consequently, we decided to artificially increase the cell density of a BIPR reaction by pelleting and resuspending an overnight culture into a reduced volume of fresh media prior to the experimental initiation. In conjunction with this, isopropyl β-d-1-thiogalactopyranoside (IPTG) was added to the reaction culture to induce luminescence overexpression within the bacteria. It is important to note that both processes strain the viability of the culture, and so balancing the nutrient requirement was needed to maintain the heightened densities of viable bacteria over the duration of a BIPR run.

Running the BIPR Experiment

With the aforementioned conditions in mind, our group was able to achieve productive catalysis and oxidative bleaching of methylene blue at concentrations up to ~1g/L of organic substrate over the course of 24 hours (Figure 12). *E. coli* cells expressing *ilux* were grown overnight at 37°C in 160mL of Luria broth (LB) containing 50µg/mL ampicillin. Prior to the addition of methylene blue and GCN, the culture was pelleted and resuspended in 80mL of fresh media. The overexpression of *ilux* was induced using 100µM of IPTG upon resuspension. The reaction itself was conducted at 37°C with shaking and the rigorous exclusion of external sources of light.

Figure 12

Oxidative Decomposition of Methylene Blue Using BIPR

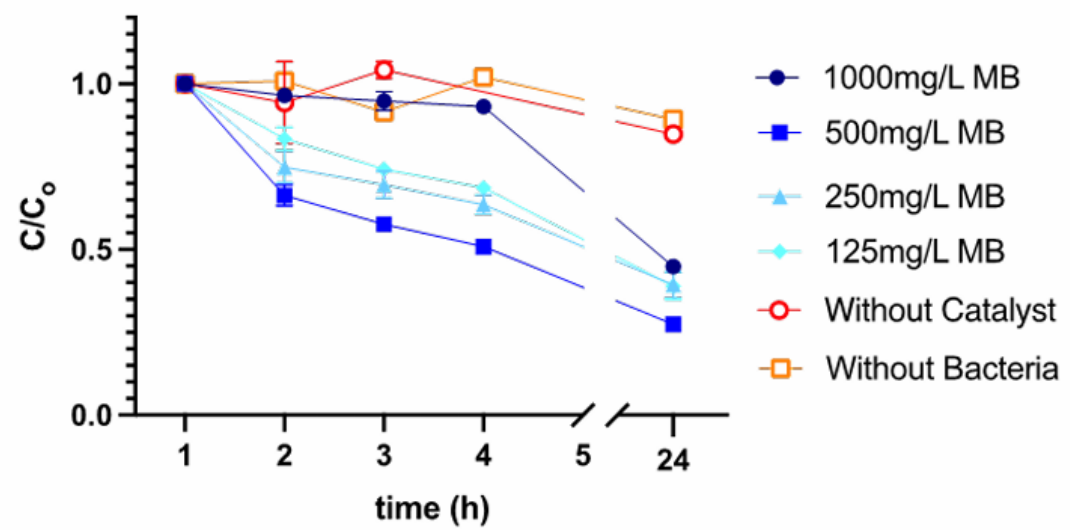

Note. This reaction was conducted over the course of 24 hours in the presence of GCN (200mg) and varied initial concentrations of dye. C_0 and C respectively represent the initial concentration and concentration at time "t" of methylene blue.

With BIPR successful in decomposing methylene blue under these conditions, I sought to advance the concept of using bioluminescent bacteria as a light source for photoredox reactions. My thesis research focused on discovering and understanding the driving forces of bacterially mediated photocatalysis.

Chapter 2

Elucidating the Mechanism of BIPR

Despite achieving BIPR, the exact mechanism responsible for the decomposition of methylene blue has avoided us. Radicals in the form of reactive oxygen species (ROS) are commonly known to be responsible for GCN-catalyzed reactions, yet the exact mechanism of how these species remains unknown. In water, the only possible photogenerated active species are holes and ROSs such as hydroxyl (•OH) radicals, superoxide ($\bullet O_2^-$) / ($\bullet HO_2^-$) radicals, hydrogen peroxide, and O_2 (Figure 13). Specific for the ROSs of the hydroxyl and superoxide radicals, it is known that they are generated via oxidation reactions in the valence band (VB) and reduction reactions in the conduction band (CB) respectively. It has been shown that the oxidation reaction in the VB between the photon-generated, positive hole (h+) and aromatic molecules can simultaneously generate hydrogen peroxide (H_2O_2)[17], displaying further advantages in the photocatalytic application of GCN. It is important to note that H_2O_2 is an oxidant that can generate additional ROS, namely the •OH radical. As seen in Figure 13, there are two possible reactions that can occur to produce hydrogen peroxide, sequential equation **C** and **D**, and the double electron transfer of equation **E**. Of these two equations, it should be noted that the sequential reaction process is more likely to occur in bulk-GCN while the double electron equation is more likely to occur in mesoporous GCN. Regardless, both equations are possible between both species of catalyst and have been identified as such.[17]

Figure 13

Diagram of Possible Radicals Produced by GCN

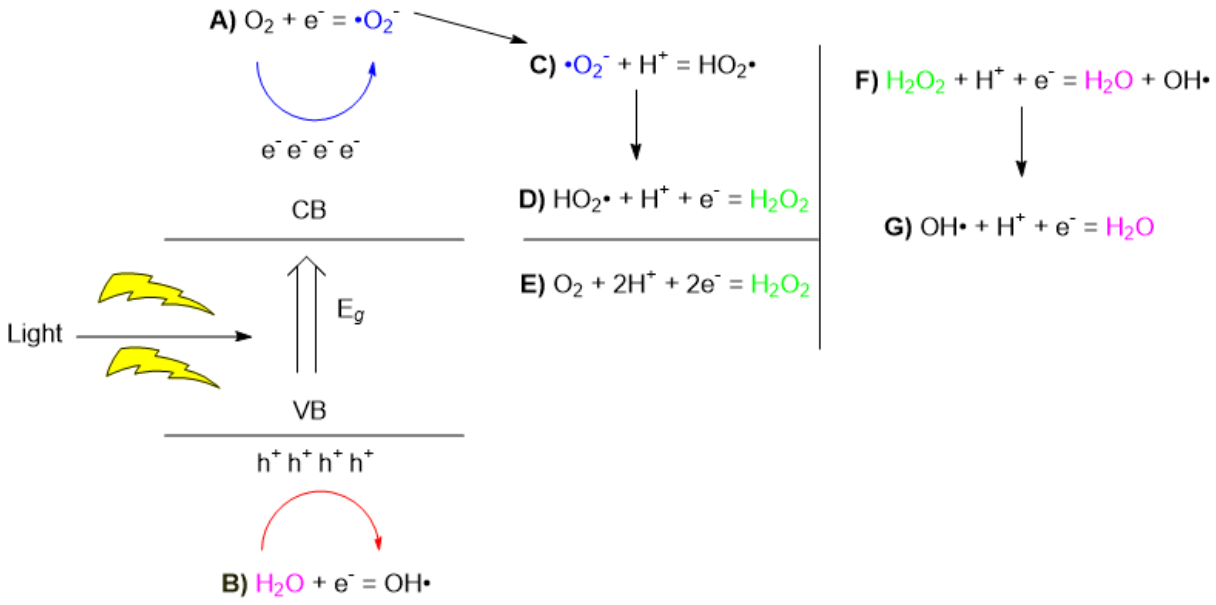

Note. Equations **A** and **B** show the reduction and oxidation processes to produce superoxide and hydroxyl radicals, respectively. Equation **C** shows the procurement of $HO_2\bullet$ and its subsequent transition to hydrogen peroxide via SET. Equation **E** is a double electron transfer that occurs with molecular oxygen to also produce hydrogen peroxide. Equations **F** and **G** display the degradation of hydrogen peroxide towards water and the hydroxyl radical and how the radical can also undergo SET to generate water back into solution.

Of the active species possible in solution with water, hydroxyl and superoxide radicals seemed the most likely candidates in driving the photocatalytic activity of GCN. To test each radical, I decided to use molecular scavengers specific to hydroxyl and

superoxide species. Tert-butyl alcohol was employed as the quencher for hydroxyl radicals, while parabenzoquinone was used as the quencher for superoxide radicals.

Tert-Butyl Alcohol and Parabenzoquinone as Radical Quenchers

Introduction to Tert-Butyl Alcohol

Figure 14

Chemical Structure of Tert-Butyl Alcohol

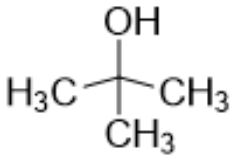

One of the most reactive and potent free radicals in natural photochemical processes is the hydroxyl radical (•OH), with a one-electron reduction potential of 2.33V.[18] One of the most prevalent scavengers for •OH is tert-butyl alcohol (TBA) (Figure 14). This molecule is commonly employed to determine the contribution of •OH to oxidative reactions. TBA has a reaction rate constant of 6×10^8 M^{-1} s^{-1} with •OH,[18] allowing TBA to outcompete other reactants and be completely scavenge any •OH radicals in solution. Even if other products form with TBA and •OH, these minor

products are considered inert and will not partake in redox reactions.[18] Each of these factors combined makes TBA an enticing quencher for •OH.

Introduction to Parabenzoquinone

Figure 15

Chemical Structure of Parabenzoquinone

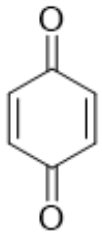

Superoxide ($•O_2^-$) is generated from molecular oxygen in atmospheric aqueous solutions.[19] As one of the most prominent ROS in aqueous environments, $•O_2^-$ is capable of diverse chemical processes as a reducing agent.[19] Parabenzoquinone (PBQ) (Figure 15) is frequently used as a $•O_2^-$ quencher due to its rate constant range of $10^8 \sim 10^9$ L mol^{-1} s^{-1}, allowing PBQ to easily quench the radical in aquatic systems.[19] As a common molecule used to quench $•O_2^-$, PBQ was employed to evaluate the impact of $•O_2^-$ in MB decomposition.

Quenching Experiments With Methylene Blue

To evaluate the effects of each radical on the decomposition of MB, four total standard 20mL scintillation vials were used with each vial containing 2.5mg of mpg-GCN and 20mL of methylene blue (20mg/L). 300mM of TBA and 0.1mM of PBQ were added to their respective vessels with two controls present to allow comparison. One control was allowed exposure to the 150W incandescent lightbulb, while the other was excluded from any light source.

Figure 16

Quenching of Methylene Blue Degradation

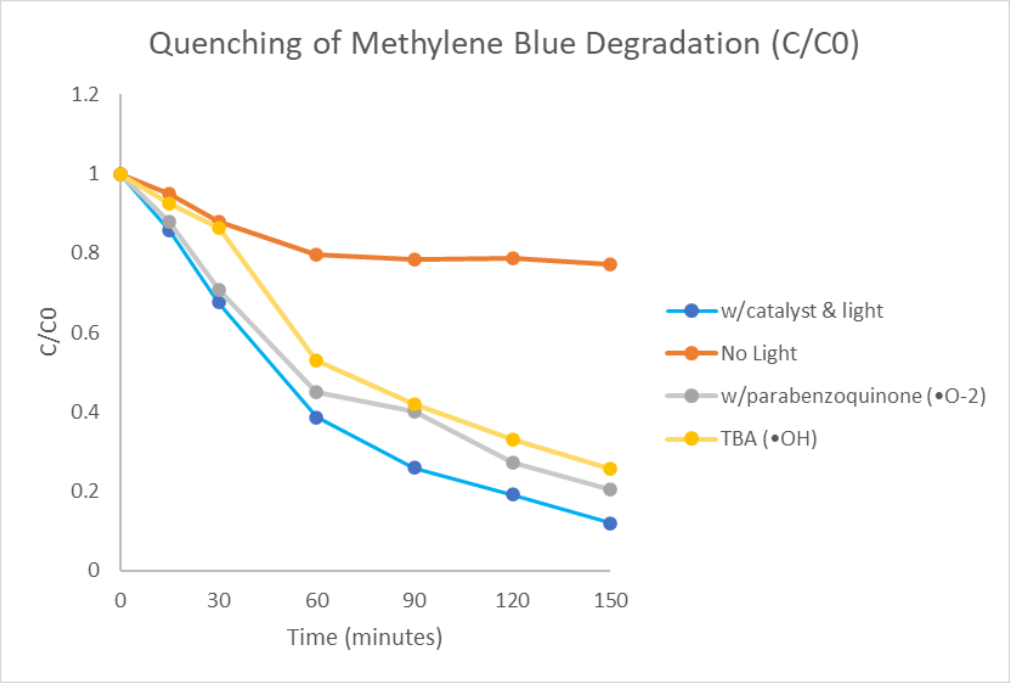

Note. This reaction was conducted over the course of 150 minutes in the presence of GCN (2.5mg), methylene blue (20mL of 20mg/L), tert-butyl alcohol (450µL of 300mM)

and parabenzoquinone (150µL of 10mM). To make up for the difference in volume for each scintillation vial, volumes of diH_2O were added to bring each vessel to a total volume of 20.45mL. C_0 and C respectively represent the initial concentration and concentration at time "t" of methylene blue.

As shown in Figure 16, TBA shows a quenching effect on the oxidative bleaching of MB up to the 30-minute mark. Thereafter, the bleaching of MB continues in accordance with the GCN control. Our group hypothesizes this initial quenching process of MB occurs due to a propagation of hydroxyl radicals in solution eventually outcompeting TBA over time. The action of PBQ during this experiment displays a slightly increased degradation of MB over the first 30 minutes and then a subsequent "slowing" of this activity afterwards. Overall, what this data suggests is that the hydroxyl radical is an active component in the degradation of methylene blue while superoxide is not.

Further Characterization of the Quenchers

To further evaluate these results, similar experiments were conducted with the concentrations of scavengers increased to further characterize their quenching activity under similar conditions. For both PBQ and TBA, two and ten times the concentration of each were into 20mL scintillation vial with 20mL of MB (20mg/L) and 2.5mg of mpg-GCN. The results for the quenching experiment using increased concentrations of TBA can be seen in Figure 17. The data reaffirms the initial quenching activity of TBA on MB degradation over the first 30 minutes further confirming our radical propagation theory.

The results for the quenching experiment using increased concentrations of PBQ can be seen in Figure 18 and display a peculiar trend in the increasing concentrations of the quencher. Unexpectedly, increasing the concentration of PBQ also increases the speed in which MB is degraded. This activity calls into question the viability of PBQ as a quencher and its aptitude in quenching superoxide radicals.

Figure 17

Quenching of Methylene Blue With Increased Concentrations of TBA

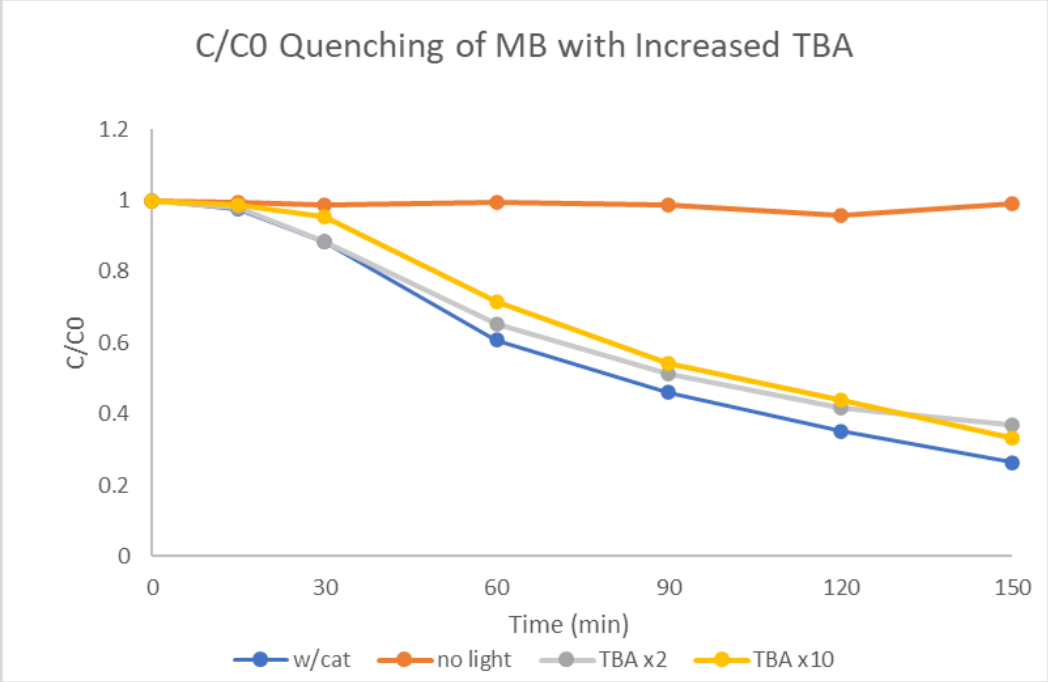

Note. This reaction was conducted over the course of 150 minutes in the presence of GCN (2.5mg), methylene blue (20mL of 20mg/L), and tert-butyl alcohol (450µL of 600mM and 450µL of 3000mM). To make up for the difference in volume for each scintillation vial, volumes of diH_2O were added to bring each vessel to a total volume of

20.45mL. C_0 and C respectively represent the initial concentration and concentration at time “t” of methylene blue.

Figure 18

Quenching of Methylene Blue With Increased Concentrations of PBQ

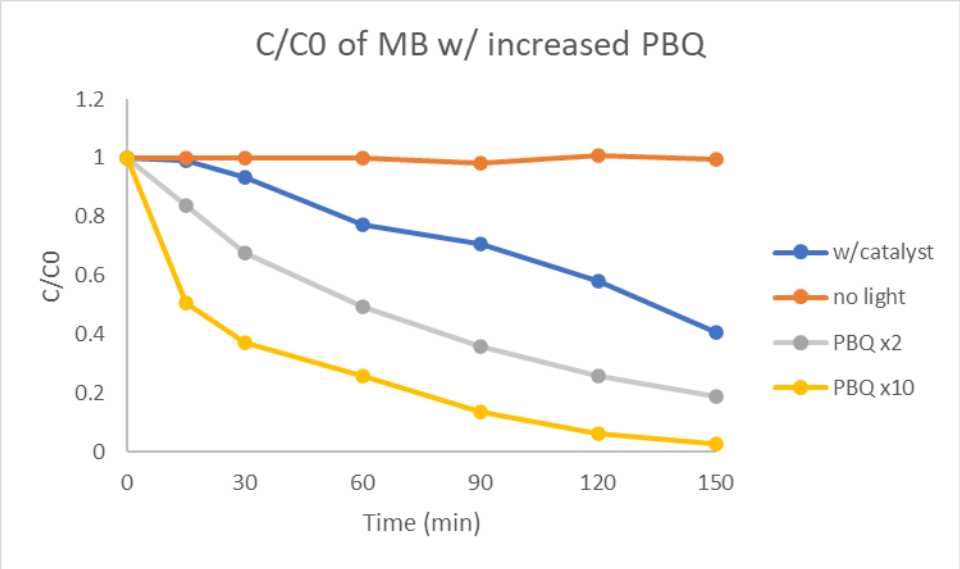

Note. This reaction was conducted over the course of 150 minutes in the presence of GCN (2.5mg), methylene blue (20mL of 20mg/L), and parabenzoquinone (150µL of 20mM and 150µL of 100mM). C_0 and C respectively represent the initial concentration and concentration at time “t” of methylene blue. To make up for the difference in volume for each scintillation vial, volumes of diH_2O were added to bring each vessel to a total volume of 20.15mL.

Understanding the Nature of Parabenzoquinone

To further investigate and characterize the increased bleaching activity of PBQ, the doubled concentrations of PBQ were reutilized. As seen in Figure 19, the results indicate that in the presence of light, parabenzoquinone can indeed increase the rate at which methylene blue can be degraded. Even when parabenzoquinone is not in solution with mpg-GCN, the trend at which methylene blue is degraded follows that of a control without parabenzoquinone or GCN catalyst. Other literature reports this startling discovery in which PBQ is capable of being easily reduced to generate a semiquinone radical (Figure 20A).[20] This then allows the PBQ radical to trap electrons in the conduction band thereby obstructing electron-hole recombination and leaving the hole open to oxidize water to •OH (Figure 20B). We can then conclude that the "catalytic" activity of PBQ we observed was due to its quinone structure and innate ability to produce further radicals.

Figure 19

Characterization of Parabenzoquinone

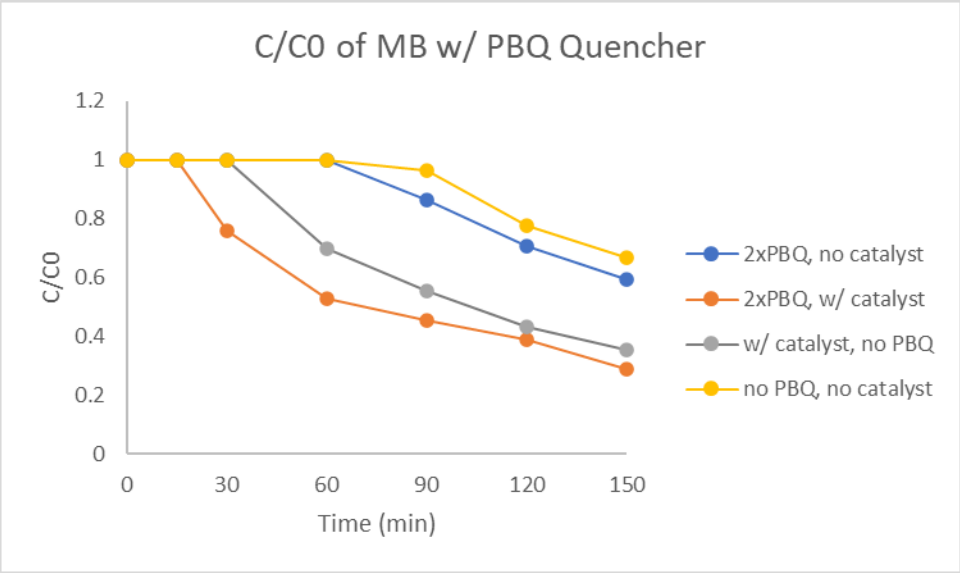

Note. This reaction was conducted over the course of 150 minutes in the presence of GCN (2.5mg), methylene blue (20mL of 20mg/L), and parabenzoquinone (150µL of 20mM). C_0 and C respectively represent the initial concentration and concentration at time "t" of methylene blue. To make up for the difference in volume for each scintillation vial, volumes of diH_2O were added to bring each vessel to a total volume of 20.15mL.

Figure 20

Reaction Scheme for Increased Hydroxyl Radical Production From Parabenzoquinone

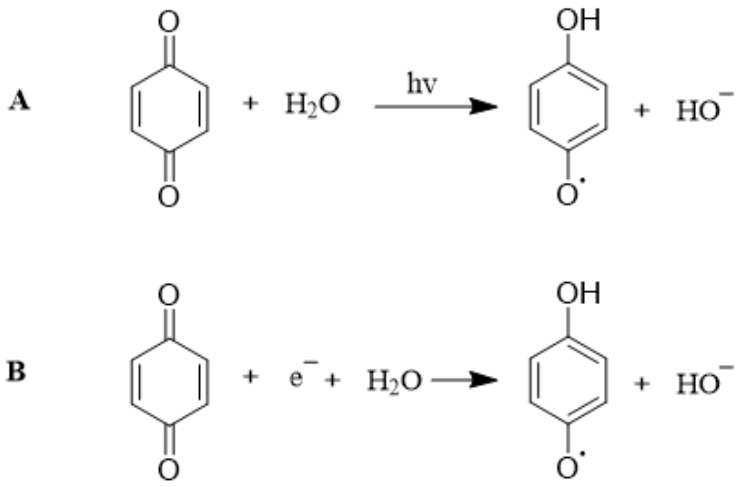

Quantifying Hydroxyl Radicals Using Terephthalate

Following the confirmation that •OH is indeed an active component in the degradation of methylene blue, I next decided to pursue quantification of the hydroxyl radical produced in solution by the mpg-GCN catalyst using disodium terephthalate (TPA) as a chemical probe (Figure 21).

Figure 21

Chemical Structure of Terephthalate and Hydroxyterephthalate

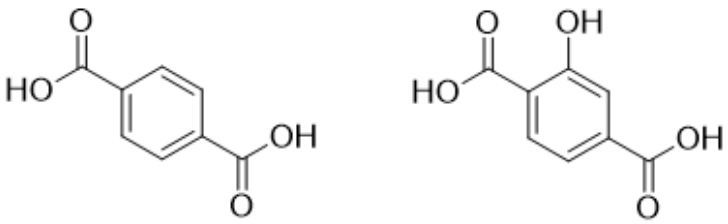

TPA is a non-fluorescent molecule and reacts selectively with •OH to generate hydroxyterephthalate (hTPA), a fluorescent molecule. This reaction would therefore allow for the easy detection and quantification of hTPA via fluorometer. Experimentally, this proved difficult due to detection limitations with the fluorometer, and results depict negligible hydroxyl formation from the mesoporous catalyst (Figure 22). This suggests that mpg-GCN does not form •OH in an aqueous environment, however, all other previous results dispute this point.

To define this seemingly errant result I decided to use our metal-containing GCN catalysts under the exact same conditions. Theoretically, mpg-GCN should produce •OH radicals and by using other catalysts we could attempt to compare their activity. As seen in Figure 23, the fluorometer revealed that all GCN catalysts produced a negligible amount of •OH, all except the iron doped GCN (Fe-GCN). The lack of •OH production from each other catalyst supports the previous study, however, the marked activity of Fe-GCN shows otherwise. In literature, Fe-GCN is shown to be capable of directly oxidizing

benzene to phenol when in a biphasic water-H_2O_2/acetonitrile medium in a stirred, self-pressurized glass reactor.[9] Additionally, it is reported that the oxidative function of Fe-GCN is capable of occurring in the dark, but is accelerated by photoredox catalysis.[9] The activity of Fe-GCN is known to occur from the binding and subsequent reduction of H_2O_2 to •OH.[9] With this information in mind, it is possible that mpg-GCN does not progress methylene blue degradation via •OH generation.

Figure 22

Detection of Hydroxyl Radicals by TPA

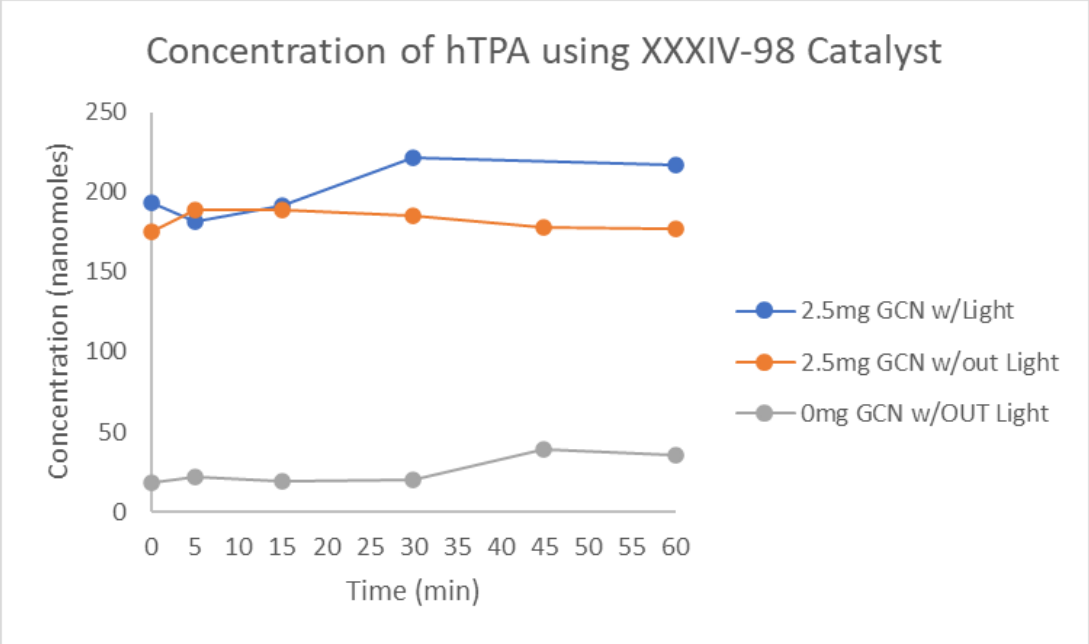

Note. This reaction was conducted over the course of 60 minutes in the presence of GCN (2.5mg) and terephthalate (20µL of 300nM).

Figure 23

Hydroxyl Radicals Produced Using Different GCN Catalysts

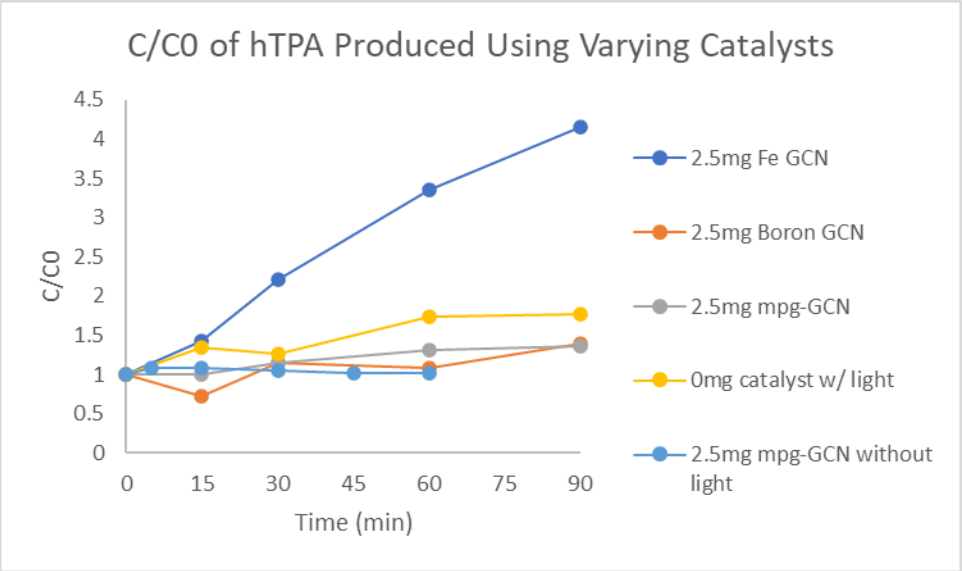

Note. This reaction was conducted over the course of 90 minutes in the presence of various doped-GCN catalysts (2.5mg) and terephthalate (20µL of 300nM).

Terephthalate as a Radical Quencher

The capacity in which •OH specifically reacts with terephthalate closely resembles the quenching activity of tert-butyl alcohol. This similarity led me to believe that TPA could be used as a quencher for MB. This idea was tested using standard 20mL scintillation vials, to which I added 20mL of MB (20mg/L), 2.5mg of mpg-GCN, terephthalate, and each quencher used previously. Figure 24 shows the results of this experiment, which was evaluated using a UV-Vis spectrophotometer.

Figure 24

Quenching Methylene Blue Degradation Using All Quenchers

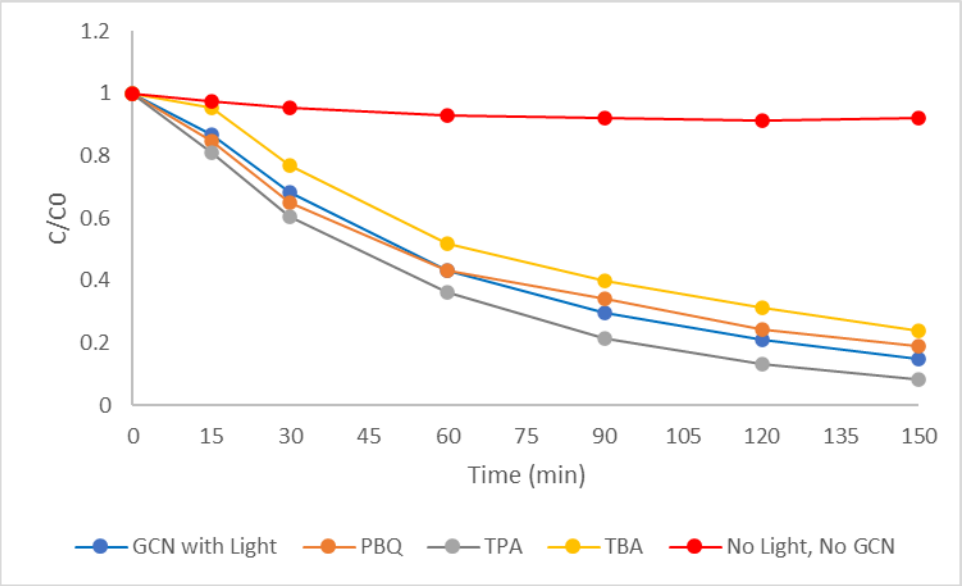

Note. This reaction was conducted over the course of 150 minutes in the presence of mpg-GCN (2.5mg), methylene blue (20mL of 20mg/L), tert-butyl alcohol (450µL of 300mM), parabenzoquinone (150µL of 10mM), and terephthalate (20µ of 300nM). To make up for the difference in volume for each scintillation vial, volumes of diH_2O were added to bring each vessel to a total volume of 20.45mL. C_0 and C respectively represent the initial concentration and concentration at time "t" of methylene blue.

Results indicated that TPA did not quench the reaction like that of TBA, instead showing a pronounced degradative effect like that of PBQ. Due to time constraints, I was unable to further investigate this interaction, however, when looking at the structure of TPA, it resembles that of PBQ. The comparable structures of both molecules lead me to

believe that TPA has a similar quinone-like activity to that of PBQ in which it can be reduced to produce a radical complex capable of increasing hydroxyl production. As of this time I have not found any literature detailing this unique action with mpg-GCN. However, this degradative action could potentially explain the lack of discernible •OH detection if TPA increases •OH production beyond the limits of what is detectable by the fluorometer. Additionally, presuming that a TPA-derived molecule can hinder electron-hole recombination in the conduction band of GCN, there would be a lack of available TPA to react with •OH and generate hTPA. Nonetheless, such an action by a molecule quencher is noteworthy and of great interest for future use in a GCN-mediated photoredox cycle.

Conclusion

My research has concentrated on the identification and quantification of the reactive radical species that drive the process of bioluminescent-induced photoredox reactions (BIPR). Current data reinforces the difficulty I have had in detecting hydroxyl radicals via fluorometer, especially in solution with MB, a fluorescent molecule itself. The identification of the forces that drive BIPR is paramount to understanding the applicability of it to future reactions. It should be noted that the evaluation of radical species is only accomplished via electron paramagnetic resonance (EPR), electron spin resonance (ESR), probe methods, or quenching methods. I made use of quenching and probe techniques in an attempt to detect, identify, and quantify the free radicals that I thought were possible in an aqueous environment, In the future, to properly conduct the quenching study, all ROS present in solution must be identified with an EPR or ESR machine. This would allow researchers to better understand the factors involved within

the environment of the BIPR reaction and plan routes to quench each radical that is formed in solution.

Complications With Quenching Studies

However, it should be noted that quenching studies are complicated and can produce invalid results based on several factors. Some of the issues with quenching include anions, dissolved organic compounds, and the pH of water in solution.[21] I did not factor these potential problems into account while running these experiments and resultingly, I was unable to detect the ROS species that I had thought were responsible for the photoredox of BIPR.

To summarize the issues of quenching studies, various particles or molecules in water have the potential to inhibit the degradation of organic pollutants via disruption of the composition of substrates and can even inhibit the redox potential of ROSs.[21] These interfering species are known to disrupt the surface properties of a catalyst and thus decrease the production of ROS,[21] a potential explanation for the lack of radicals detected in my research. As stated previously, the pH of these quenching studies was something that I did not consider. The pH of photoredox reactions can affect the reaction rate of scavengers and ROS, and in some cases, can generate new RS.[21] The possibility for new and unidentified radicals forming in solution is yet another reason that EPR or ESR machines should be utilized in future experiments.

More factors to consider when running a quenching study is whether a quencher is inoculated before or after the launch of a catalytic reaction.[21] Adding in a high enough concentration of quenchers before catalytic initiation can cause the active sites of

catalysts to be blocked. In my quenching studies, I inoculated each quencher at the initiation of the lightbulb, which should have overcome this issue. Despite this fix however, I question whether the methylene blue should be equilibrated with the GCN catalyst prior to the initiation of photoredox. Similar to an increased amount of quenchers inhibiting the catalyst, perhaps the adsorption of MB to GCN at a high enough concentration "inhibits" the acting role of the quencher. An experiment using adding both MB and the quencher at the same time could dispute this. Additionally, the optimization of catalyst, dye, or quencher amount should be taken into account.

To properly evaluate superoxide, future studies could utilize hydroethidine (HE) as a superoxide radical probe. Using HPLC and LC-MS techniques, 2-hydroxyethidium can be specifically detected to detect the presence of a superoxide radical,[22] making HE an enticing molecular probe for further testing with radicals produced by GCN. Due to concerns with the toxicity of HE, it was decided to avoid this method of radical detection, however, literature studies still demonstrate the superiority of this method of detection.[22-24]

Parabenzoquinone was found to be unsuccessful as a superoxide quencher in my study, and instead further increased the degradation of methylene blue. In parallel to this, TPA did not quench the degradative oxidation of methylene blue. While I was unable to further characterize TPA's ability to accelerate MB degradation, results imply that increasing the concentration of TPA would display this activity. Herein it appears that quinone-like structures possess the capability to increase the rate at which MB can be degraded. Future experiments could evaluate the use of other similar molecules for potential use in increasing the oxidative potential of GCN as additives.

With the development of multiple improved catalysts following our initial tests for BIPR-driven organic synthesis using bulk GCN, it is important to note that these catalysts were never tested. Future testing in BIPR could examine the ability of these doped GCN catalysts to oxidate aminobenzenes and THQ. Also important to discuss is the nature of these heteroatom catalysts. Despite being doped with other compounds, these catalysts would still be considered as "bulk" catalysts due to the small specific surface area of each. For Fe-GCN, literature reports the use of SBA-15, a widely used mesoporous catalyst support that is capable of increasing GCN's surface area.[9] This could be accomplished by copolymerizing dicyanamide and the "doping molecule" (for Fe-GCN, $FeCl_3$; for Na-GCN, Na_2CO_3; etc.).

Following up on this concept, all current and future synthesized catalyst materials should be characterized to assert whether the desired catalyst was properly formulated. To achieve this, XRD patterns can be used to confirm the mesostructure of porous catalysts, TEM images could confirm the surface structure of the catalyst, and elemental mapping images could be used to give evidence that the proper catalyst was formulated.

Closing Remarks

Overall, this study highlights the success of a bacterially mediated photoredox reaction in degrading organic dye. I have identified hydroxyl radicals as the most probable ROS in driving BIPR and I have inadvertently discovered the potential use of parabenzoquinone and disodium terephthalate as chemical additives to increase the rate in which hydroxyl radicals form in solution with GCN.

References

(1) Zhang, B.; Sun, L. Artificial photosynthesis: opportunities and challenges of molecular catalysts. *Chemical Society reviews* **2019**, *48* (7), 2216-2264. DOI: 10.1039/c8cs00897c.

(2) Prier, C. K.; Rankic, D. A.; MacMillan, D. W. C. Visible Light Photoredox Catalysis with Transition Metal Complexes: Applications in Organic Synthesis. *Chemical reviews* **2013**, *113* (7), 5322-5363. DOI: 10.1021/cr300503r.

(3) Savateev, A.; Antonietti, M. Heterogeneous Organocatalysis for Photoredox Chemistry. *ACS catalysis* **2018**, *8* (10), 9790-9808. DOI: 10.1021/acscatal.8b02595.

(4) Kandoth, N.; Pérez Hernández, J.; Palomares, E.; Lloret-Fillol, J. Mechanisms of photoredox catalysts: the role of optical spectroscopy. *Sustainable energy & fuels* **2021**, *5* (3), 638-665. DOI: 10.1039/d0se01454k.

(5) Lee, J.; Müller, F.; Visser, A. J. W. G. The Sensitized Bioluminescence Mechanism of Bacterial Luciferase. *Photochemistry and photobiology* **2019**, *95* (3), 679-704. DOI: 10.1111/php.13063.

(6) Gregor, C.; Gwosch, K. C.; Sahl, S. J.; Hell, S. W. Strongly enhanced bacterial bioluminescence with the ilux operon for single-cell imaging. *Proceedings of the National Academy of Sciences - PNAS* **2018**, *115* (5), 962-967. DOI: 10.1073/pnas.1715946115.

(7) Brodl, E.; Winkler, A.; Macheroux, P. Molecular Mechanisms of Bacterial Bioluminescence. *Computational and structural biotechnology journal* **2018**, *16*, 551-564. DOI: 10.1016/j.csbj.2018.11.003.

(8) Zhang, Q.; Chen, Y.; Zhao, C.; Yang, X.; Chen, Z. Facile regeneration of oxidized porous carbon nitride rods by the de-aromatization of the heptazine network in bulk g-CN. *Inorganic chemistry frontiers* **2022**, *9* (6), 117-1114. DOI: 10.1039/d1qi01607e.

(9) Chen, X.; Zhang, J.; Fu, X.; Antonietti, M.; Wang, X. Fe-g-C3N4-Catalyzed Oxidation of Benzene to Phenol Using Hydrogen Peroxide and Visible Light. *Journal of the American Chemical Society* **2009**, *131* (33), 11658-11659. DOI: 10.1021/ja903923s.

(10) Guo, X.; Rao, L.; Wang, P.; Zhang, L.; Wang, Y. Synthesis of Porous Boron-Doped Carbon Nitride: Adsorption Capacity and Photo-Regeneration Properties. *International journal of environmental research and public health* **2019**, *16* (4), 581. DOI: 10.3390/ijerph16040581.

(11) Li, H.; Wang, L.; Liu, Y.; Lei, J.; Zhang, J. Mesoporous graphitic carbon nitride materials: synthesis and modifications. *Research on chemical intermediates* **2016**, *42* (5), 3979-3998. DOI: 10.1007/s11164-015-2294-9.

(12) Mallikarjuna, K.; Kumar, M. K.; Kim, H. Synthesis of oxygen-doped-g-C3N4/WO3 porous structures for visible driven photocatalytic H2 production. *Physica. E, Low-dimensional systems & nanostructures* **2021**, *126*, 114428. DOI: 10.1016/j.physe.2020.114428.

(13) Phoon, B. L.; Lai, C. W.; Pan, G.-T.; Yang, T. C. K.; Juan, J. C. Highly Mesoporous g-C3N4 with Uniform Pore Size Distribution via the Template-Free Method to Enhanced Solar-Driven Tetracycline Degradation. *Nanomaterials (Basel, Switzerland)* **2021**, *11* (8), 2041. DOI: 10.3390/nano11082041.

(14) Prabakaran, E.; Velempini, T.; Molefe, M.; Pillay, K. Comparative study of KF, KCl and KBr doped with graphitic carbon nitride for superior photocatalytic degradation of methylene blue under visible light. *Journal of materials research and technology* **2021**, *15*, 6340-6355. DOI: 10.1016/j.jmrt.2021.10.128.

(15) Yan, L.; Gao, H.; Chen, Y. Na-Doped Graphitic Carbon Nitride for Removal of Aqueous Contaminants via Adsorption and Photodegradation. *ACS applied nano materials* **2021**, *4* (8), 7746-7757. DOI: 10.1021/acsanm.1c01035.

(16) Wang, H.; Zhang, J.; Wang, P.; Yin, L.; Tian, Y.; Li, J. Bifunctional copper modified graphitic carbon nitride catalysts for efficient tetracycline removal: Synergy of adsorption and photocatalytic degradation. *Chinese chemical letters* **2020**, *31* (10), 2789-2794. DOI: 10.1016/j.cclet.2020.07.043.

(17) Zhang, H.; Guo, L.-H.; Zhao, L.; Wan, B.; Yang, Y. Switching Oxygen Reduction Pathway by Exfoliating Graphitic Carbon Nitride for Enhanced Photocatalytic Phenol Degradation. *The journal of physical chemistry letters* **2015**, *6* (6), 958-963. DOI: 10.1021/acs.jpclett.5b00149.

(18) Gao, Z.; Zhang, D.; Jun, Y.-S. Does Tert-Butyl Alcohol Really Terminate the Oxidative Activity of •OH in Inorganic Redox Chemistry? *Environmental science & technology* **2021**, *55* (15), 10442-10450. DOI: 10.1021/acs.est.1c01578.

(19) Zhu, M.; Lu, J.; Hu, Y.; Liu, Y.; Hu, S.; Zhu, C. Photochemical reactions between 1,4-benzoquinone and O2. *Environmental science and pollution research international* **2020**, *27* (25), 31289-31299. DOI: 10.1007/s11356-020-09422-8.

(20) Schneider, J. T.; Firak, D. S.; Ribeiro, R. R.; Peralta-Zamora, P. Use of scavenger agents in heterogeneous photocatalysis: truths, half-truths, and misinterpretations. *Physical chemistry chemical physics : PCCP* **2020**, *22* (27), 15723-15733. DOI: 10.1039/d0cp02411b.

(21) Liu, W.; Lu, Y.; Dong, Y.; Jin, Q.; Lin, H. A critical review on reliability of quenching experiment in advanced oxidation processes. *Chemical engineering journal (Lausanne, Switzerland : 1996)* **2023**, *466*, 143161. DOI: 10.1016/j.cej.2023.143161.

(22) Kalyanaraman, B.; Hardy, M.; Podsiadly, R.; Cheng, G.; Zielonka, J. Recent developments in detection of superoxide radical anion and hydrogen peroxide: Opportunities, challenges, and implications in redox signaling. *Archives of biochemistry and biophysics* **2017**, *617*, 38-47. DOI: 10.1016/j.abb.2016.08.021.

(23) Nazarewicz, R. R.; Bikineyeva, A.; Dikalov, S. I. Rapid and Specific Measurements of Superoxide Using Fluorescence Spectroscopy. *SLAS discovery* **2013**, *18* (4), 498-503. DOI: 10.1177/1087057112468765.

(24) Kalyanaraman, B.; Dranka, B. P.; Hardy, M.; Michalski, R.; Zielonka, J. HPLC-based monitoring of products formed from hydroethidine-based fluorogenic probes — The ultimate approach for intra- and extracellular superoxide detection. *Biochimica et biophysica acta. General subjects* **2014**, *1840* (2), 739-744. DOI: 10.1016/j.bbagen.2013.05.008.

Appendix A

NMR Data from Initial THQ BIPR Experiments

Figure A1

NMR Data for Pure THQ

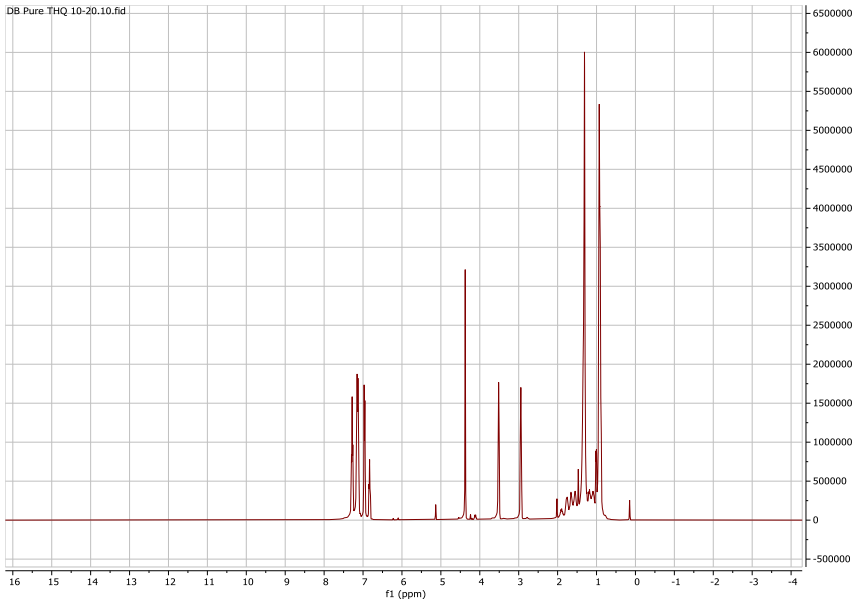

Figure A2

NMR Data for Fraction Work-up of THQ

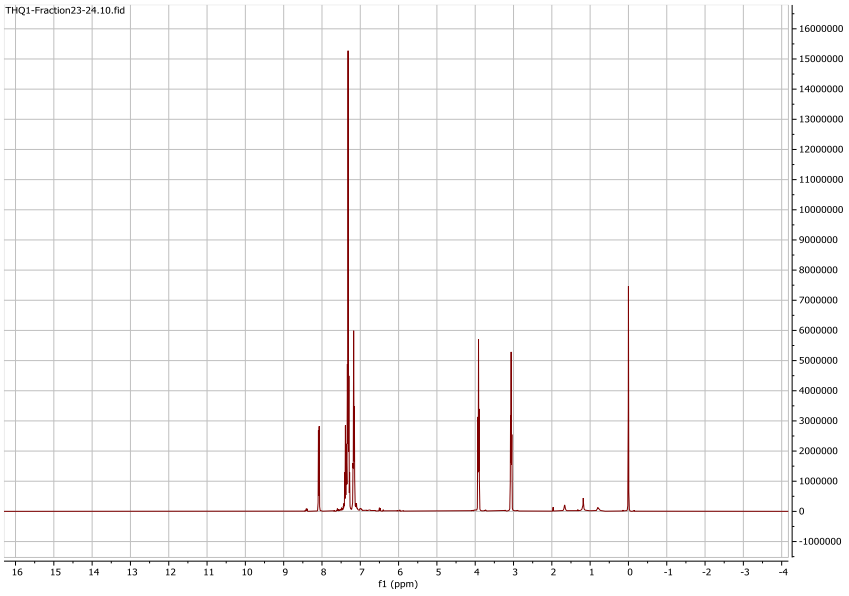

Figure A3

Crude NMR Data for Oxidation of THQ to 2-phenyl-THQ

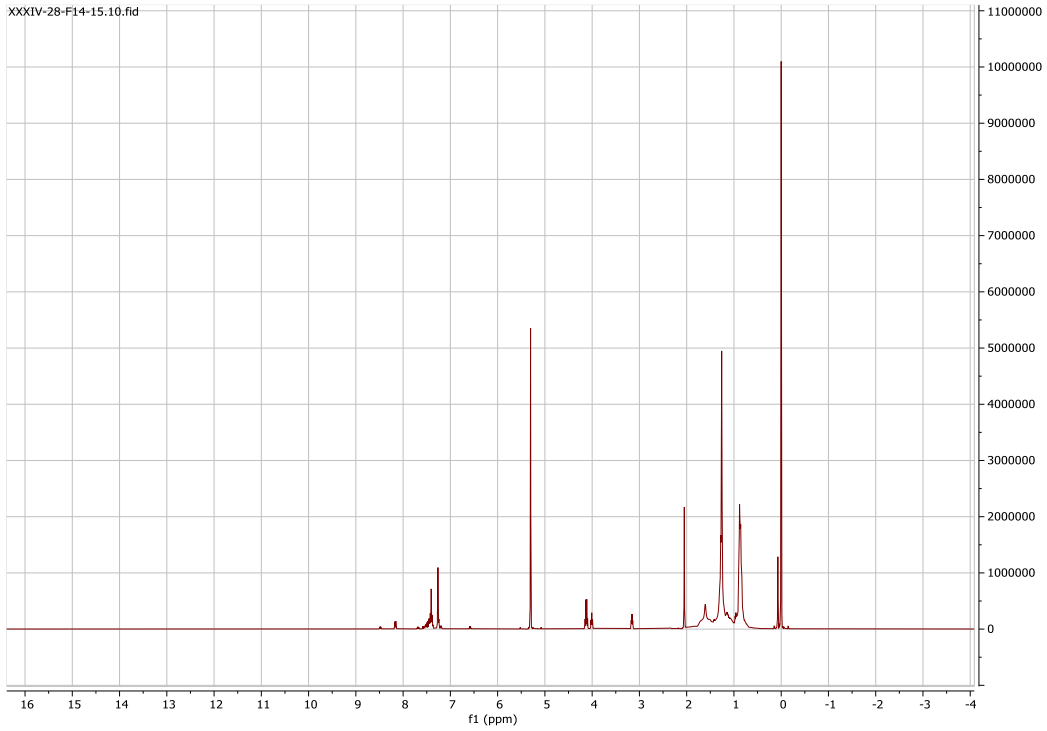

Appendix B

NMR Data for the Oxidation of Phenylmethanamine

Figure B1

NMR Data for the Oxidized Product of Phenylmethanamine

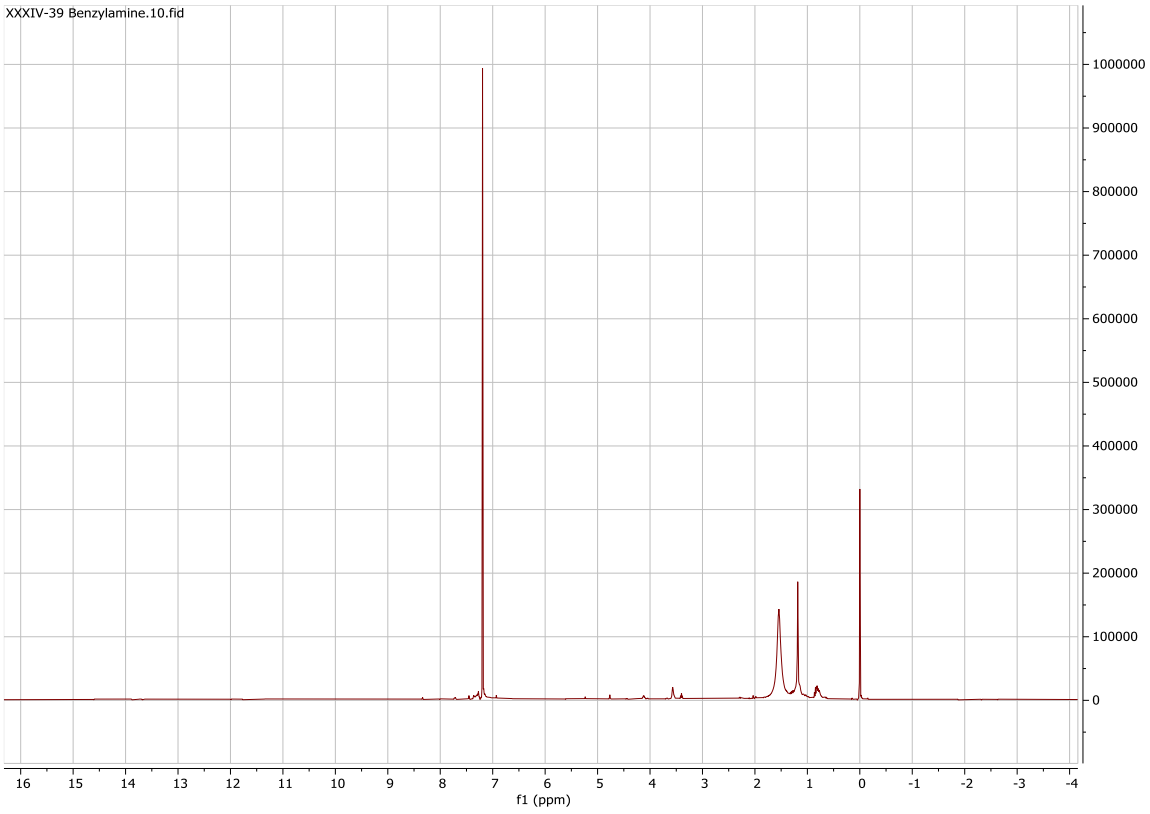

Appendix C

NMR Data for the Oxidation of N, N-Dimethyl-1-Phenylmethanamine

Figure C1

NMR for Initial N, N-dimethyl-1-phenylmethanamine Starting Product

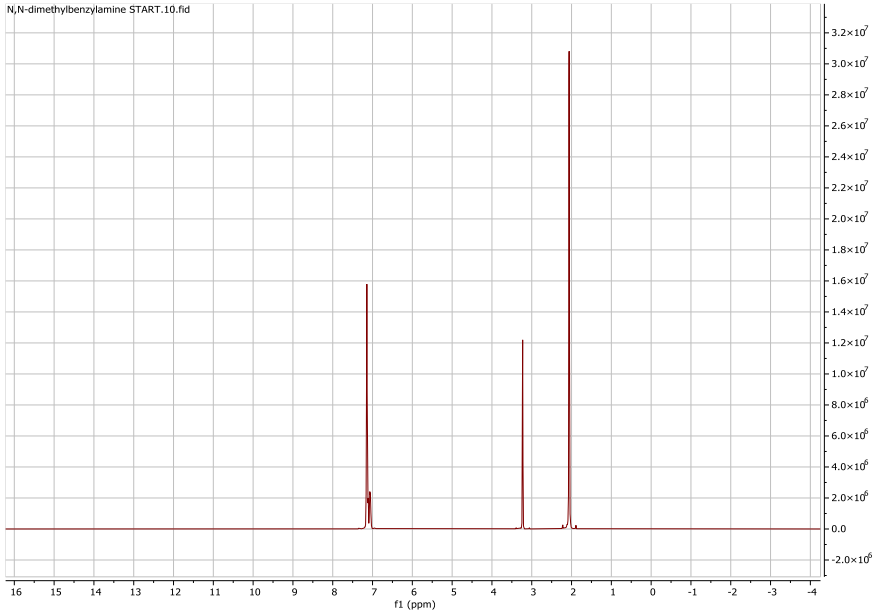

Figure C2

Crude NMR Data for N, N-dimethyl-1-phenylmethanamine

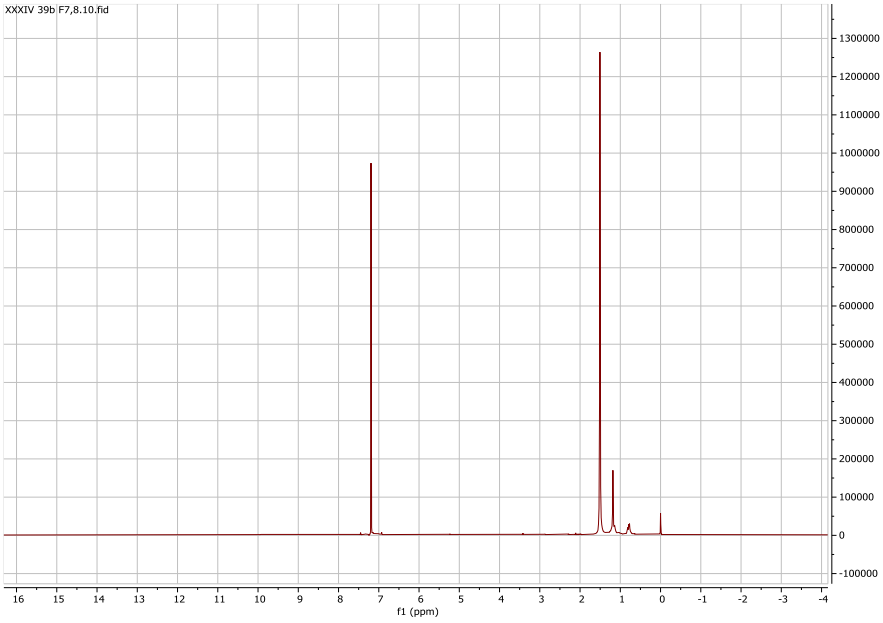

Appendix D

NMR Data for the Oxidative Coupling of Benzylamine Hydrochloride

Figure D1

NMR Data for Naturally Synthesized Benzylamine Coupling Product

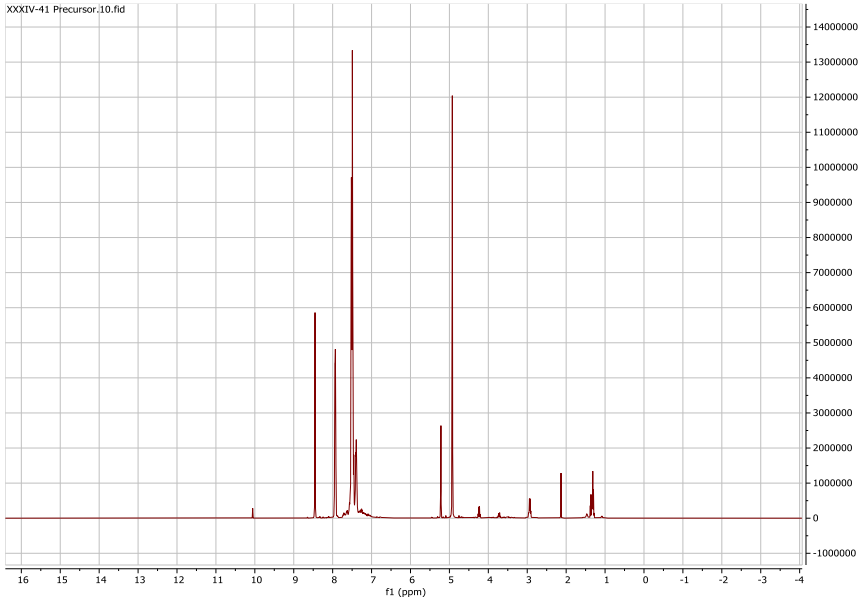

Figure D2

NMR Data for Benzylamine Product at 3.5 Hours

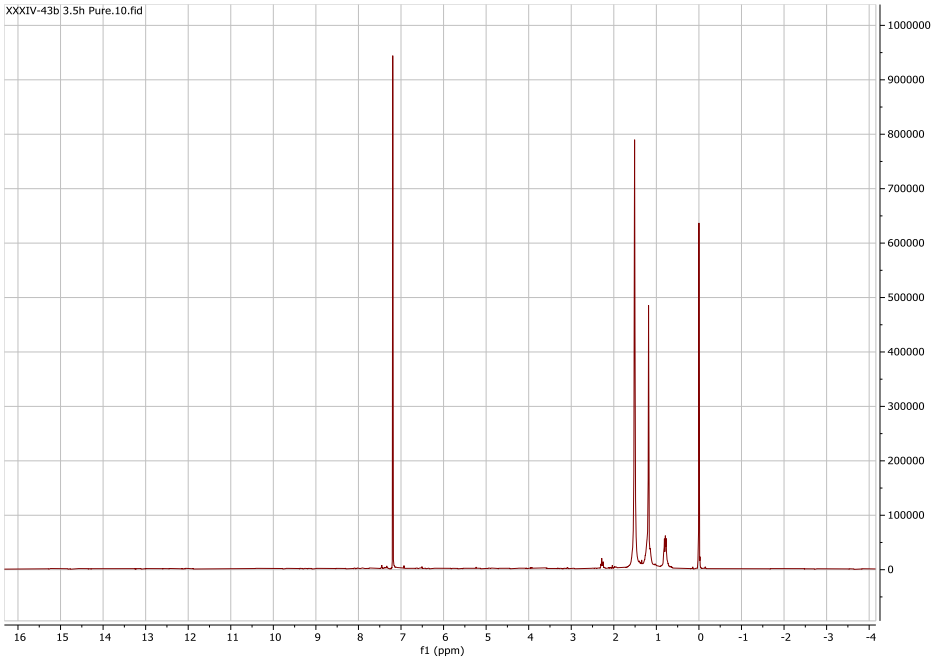

Figure D3

NMR Data for Benzylamine Product at 12 Hours

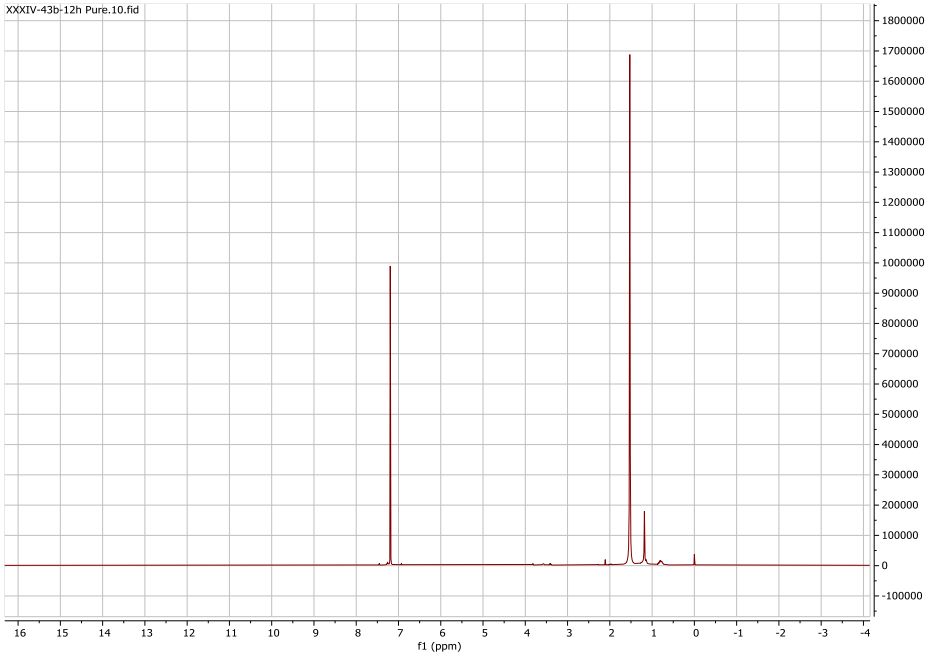

Figure D4

Crude NMR Data for Benzylamine Product at 24 Hours